IEEE Access
Multidisciplinary | Rapid Review | Open Access Journal

Received February 24, 2018, accepted March 28, 2018, date of publication April 16, 2018, date of current version May 2, 2018.

Digital Object Identifier 10.1109/ACCESS.2018.2824559

Online Estimation of State of Power for Lithium-Ion Batteries in Electric Vehicles Using Genetic Algorithm

JIAHUAN LU[1,2], ZEYU CHEN[2], YING YANG[2], AND MING LV[2]
[1]State Key Laboratory of Automotive Simulation and Control, Changchun 130025, China
[2]Northeastern University, Shenyang 110819, China

Corresponding author: Zeyu Chen (chenzy@mail.neu.edu.cn)

This work was supported in part by the Foundation of State Key Laboratory of Automotive Simulation and Control under Grant 20161106, in part by the National Natural Science Foundation of China under Grant 51607030, and in part by the Fundamental Research Funds for the Central Universities under Grant N160304001.

ABSTRACT Online estimation of the state of power (SoP) of lithium-ion batteries is crucial for both battery management system and energy management system in electric vehicles. In this paper, the approach of online estimating the SoP is investigated with a concern of the impact of the imprecise state of charge (SoC). First, the characteristics of lithium batteries under different state of health (SoH) conditions are experimented based on a typical vehicle driving cycle; then the SOP estimation algorithm using genetic algorithm (GA) is proposed to deal with the long time-scale estimation for power management application, on top of that, the sensitivity coefficient (δ) of the SoP estimation to the SoC precision is analyzed and the correlations of δ with the varying SoH, estimation time-scale are established. Finally, the presented algorithm is evaluated by a simulation study. The proposed GA-based estimation method can improve the SoP estimation accuracy by up to 7.2% in certain cases compared with the traditional Taylor method.

INDEX TERMS Electric vehicles, battery management system, state estimation, genetic algorithm.

I. INTRODUCTION

Currently, the astonishing growth of fossil fuel-dominated vehicles has put a serious impact on the environment and energy issues [1]–[4]. In this situation, electric vehicles (EVs), including battery electric vehicles (BEVs), fuel cell electric vehicles (FCEVs), hybrid electric vehicles (HEVs), and plug-in hybrid electric vehicles (PHEVs), have gradually been recognized as the highly promising developments due to their low emission and high energy efficiencies [5]–[7]. As the onboard power source of EVs, traction battery packs play an important role in improving vehicular performance, in which the LiBs are most common used battery type for the high energy density, long lifespan, low self-discharge and no memory effect [8].

The battery management system (BMS) of LiBs is in charge of providing estimations of the battery states, mainly including the SoC, SoH and SoP [9], [10]. However, precisely estimating the battery states remains a technical challenge so far because of the complex nonlinear characteristics of LiBs and their complicated application circumstance in vehicles [11]. SoP is the common used indicator of the maximum charging and discharging power capabilities of LiB, which is crucial for both the battery management and vehicle supervisory control system.

A. REVIEW OF LITERATURE

The estimation of SoP has attracted a lot of attention of researchers. The existing publications for SoP estimation are mainly divided into two categories, one is the characteristic map (CM)-based methods and the other is the equivalent circuit model (ECM)-based methods.

1) CM-BASED METHODS

This type of method is based on offline CMs stored in the BMS memory to calculate the SoP, where the offline CMs mainly contain the static interdependence among the SoP, battery states (like SoC, SoH, and temperature) and power pulse parameters (such as the estimation time-scale of the power pulse) [12]. The initial parameterization of the CMs needs to be conducted in a specific experimental environment, following the recommendations by various correlative manuals and standards. This kind of method is simple

and easily implemented. However, LiB is a nonlinear time-varying system, which characteristics strongly depend on the previous history, so the dynamic behavior cannot be accurately reflected only with the static offline CMs. Additionally, the aforementioned static interdependence involves many dimensions, which means a large storage capacity for the BMS is requisite [13]. To reduce this storage requirement, Kim *et al.* [14] used various mathematical functions to approximate the interdependence instead of the large amount of CM data.

2) ECM-BASED METHODS

ECMs use lumped-parameter circuit elements (e.g. resistors, capacitors and inductors) to describe the battery impendence characteristic. This kind of method usually relies the Taylor expansion method to estimate the model in the future time-scale, if the ECM can accurately reflect the battery dynamic behavior, the SoP estimation result can be relatively precise. Till now, this method has attracted much attention of researchers [15]–[26], to name a few, Plett [15] uses a simple ECM to calculate the SoP subject to the limitations of current, voltage and SoC, considering future variation of the open circuit voltage (OCV); Sun *et al.* [16] developed the first-order RC model to provide a much more accurate SoP prediction considering the polarization effect and different equivalent ohmic resistances; Xiong *et al.* [17] proposed a joint SoC and SoP estimator to achieve a reliable SoP prediction using an adaptive extended Kalman filter (AEKF). The above studies have made great progresses, but the lack of the mathematical proof expose an inaccurate risk of the estimation results. To solve this problem, Mellado *et al.* [27] provided a detailed mathematical proof of the proposed algorithms and adopted optimization algorithms to the prediction solution.

B. MOTIVATION AND INNOVATION

Till now, most of SoP estimation researches, in which the long time-scale of the estimation has not been well emphasized, are not specially targeted to the vehicle power management applications. In addition, the SoP estimation algorithms normally rely on the precise SoC information, however, precisely estimating the battery SoC in EVs applications is still quite difficult. Some publications focus on the joint estimating of SoC and SoP [28], [29], but there is a lack of a quantitative study on the impact of SoC estimating error on the SoP estimation.

The objective of this study is to propose an effective online SoP estimation approach of lithium batteries used in EVs power management system and analyze the influence of imprecise SoC information. Three original contributions are made:

(1) The Taylor method for SoP estimation is discussed and the impact of its remainder error is given under the varying estimation time-scale.
(2) The improved GA is employed for online estimating the battery SoP under long estimation time-scale in vehicle power management application.
(3) The impact of the imprecise SoC on the SoP estimation is analyzed quantitatively by bringing in a sensitivity coefficient. The correlations between sensitivity coefficient and its influences are disclosed.

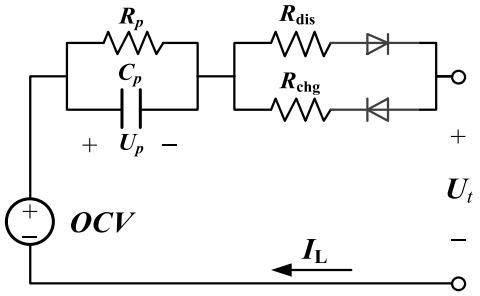

FIGURE 1. Schematic of the first-order RC model.

C. ORGANIZATION OF THE PAPER

The remainder of this paper is organized as follows: the experimental study and battery modeling are described in section 2; in Section 3, the drawback of Taylor method is discussed and the improved GA-based SoP estimation approach is proposed; the verification and evaluation of the algorithm are carried out in section 4; the influence of the SoC error on the SoP estimation under varying conditions are investigated in section 5 while the conclusions are summarized in section 6.

II. BATTERY MODELING

A. BATTERY TEST AND MODEL

First of all, the battery test is conducted to investigate the battery characteristic. In this study, we focus on the battery SoP estimation for the electric vehicle power management application, so therefore, the charging and discharging characteristic test is under the Urban Dynamometer Driving Schedule (UDDS).

The first-order RC equivalent circuit model is established, as shown in Fig. 1, in which the resistance block includes a charging ohmic resistance R_{chg} and a discharging ohmic resistance R_{dis}. The equivalent RC block is used to model the polarization effect, which contains a polarization resistance R_p and a capacitor C_p. The electrical behavior of the battery is described as:

$$\begin{cases} U_{p,k+1} = U_{p,k} e^{\frac{-\Delta t}{R_p C_p}} + \left(1 - e^{\frac{-\Delta t}{R_p C_p}}\right) R_p I_{L,k} \\ U_{t,k+1} = OCV - I_{L,k+1} R_{dis} - U_{p,k+1} \quad \text{if } I_{L,k+1} \geq 0 \\ U_{t,k+1} = OCV - I_{L,k+1} R_{chg} - U_{p,k+1} \quad \text{if } I_{L,k+1} < 0 \\ \tau = R_p C_p \end{cases} \tag{1}$$

where Δt is the sampling time interval, τ is the time constant of the RC block, and $U_{p,k+1}$, $U_{t,k+1}$ and $I_{L,k+1}$ are the polarization voltage, terminal voltage and load current at the $(k+1)$th sampling interval, respectively.

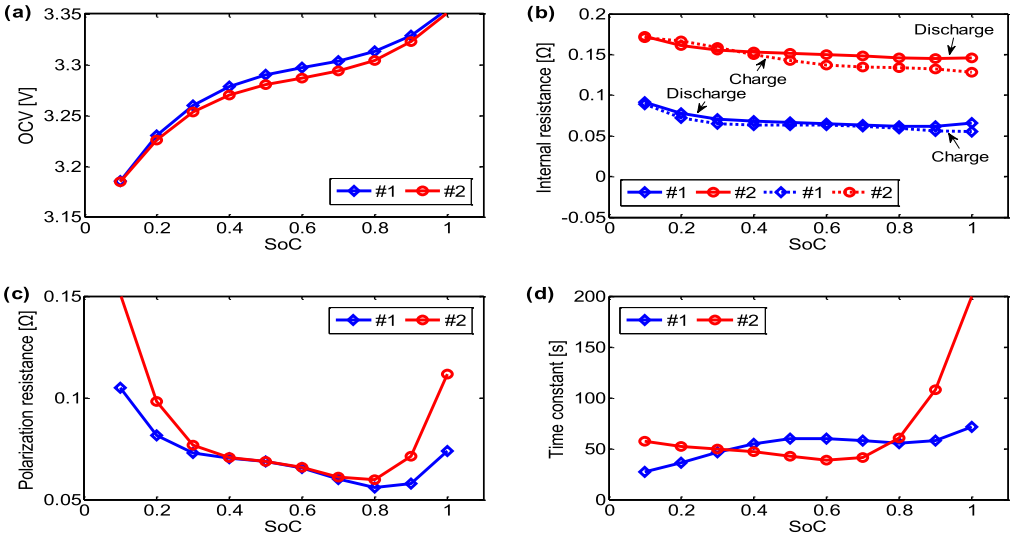

FIGURE 2. Identification results of batteries: (a) OCV; (b) internal resistance includes R_{dis} and R_{chg}; (c) polarization resistance; (d) time constant.

In this study, two lithium-ion cells with different SoH are investigated, marked as #1 and #2. Cell #1 is a health new cell with the SoH>96% while cell #2 is an aging cell with the SoH<85%. Here, the SoH is defined using the capacity degradation of the battery:

$$\text{SoH} = \frac{C}{C_{\max}} \times 100\% \tag{2}$$

where C is the present capacity from the static capacity test, and $C_{\max}$ is the nominal rated capacity.

B. PARAMETERS IDENTIFICATION

The parameters in the model vary with SoC and temperature. In this study, the impact of temperature is neglected, thus, the parameters are treated as functions of SoC, expressed by

$$\begin{cases} OCV(z) = a_1 e^{-a_2 z} + a_3 + a_4 z + a_5 z^2 + a_6 z^3 \\ R_{dis}(z) = b_1 z^4 + b_2 z^3 + b_3 z^2 + b_4 z + b_5 \\ R_{chg}(z) = c_1 z^4 + c_2 z^3 + c_3 z^2 + c_4 z + c_5 \\ R_p(z) = d_1 z^4 + d_2 z^3 + d_3 z^2 + d_4 z + d_5 \\ \tau(z) = e_1 z^4 + e_2 z^3 + e_3 z^2 + e_4 z + e_5 \end{cases} \tag{3}$$

where z is the battery SoC, and $a_1 \sim a_6$, $b_1 \sim b_5$, $c_1 \sim c_5$, $d_1 \sim d_5$ and $e_1 \sim e_5$ are coefficients that need to be identified.

The battery SoC is updated by the ampere counting approach based on the current data and sampling time interval

$$z_{k+1} = z_k - \frac{I_{L,k+1}\Delta t}{C}\eta_k \tag{4}$$

where η_k is the coulomb efficiency at the $(k+1)$th sampling interval.

The optimal parameters are obtained by the identification algorithm in minimizing the objective function:

$$\min J = \left(\sqrt{\frac{1}{M}\sum_{i=1}^{M} \left(U_{t,k} - \hat{U}_{t,k}(\hat{\theta}) \right)^2} \right) \tag{5}$$

where M is the total sample number of the experimental data, $\hat{\theta}$ is the function coefficient vector representing the estimated parameters, and $\hat{U}_{t,k}$ is the terminal voltage estimation.

The parameter identification results of the two LiB cells are given in Fig. 2 while the test valuations of the model prediction performances are shown in Fig. 3. The test results indicate that the established battery model can fit precisely with the test data where the maximum relative error of the model is less than 1.0% and the mean relative error is less than 0.12%.

III. ONLINE SoP ESTIMATION

A. FORMULATION OF THE OPTIMIZATION PROBLEM

In this section, an improved GA is employed for predicting the SoP of the battery. The SoP estimation is treated as a optimization problem to find the maximum of battery power within a certain time-scale under several constraints. The maximum battery power within a time-scale T after time k is expressed as:

$$P_{L,k+T} = \begin{cases} \text{if } I_{L,k+T} \geq 0: \\ I_{L,k+T}\left(\begin{array}{l} OCV(z_k - \dfrac{I_{L,k+T}\Delta t}{C} T\eta_d) \\ -I_{L,k+T} R_{dis}(z_k - \dfrac{I_{L,k+T}\Delta t}{C} T\eta_d) - U_{p,k+T} \end{array} \right) \\ \text{if } I_{L,k+T} < 0: \\ I_{L,k+T}\left(\begin{array}{l} OCV(z_k - \dfrac{I_{L,k+T}\Delta t}{C} T\eta_c) \\ -I_{L,k+T} R_{chg}(z_k - \dfrac{I_{L,k+T}\Delta t}{C} T\eta_c) - U_{p,k+T} \end{array} \right) \end{cases} \tag{6}$$

in which the timescale T is the time span that the maximum power could last, and $I_{L,k+T}$ is the battery load current from time k to $k+T$.

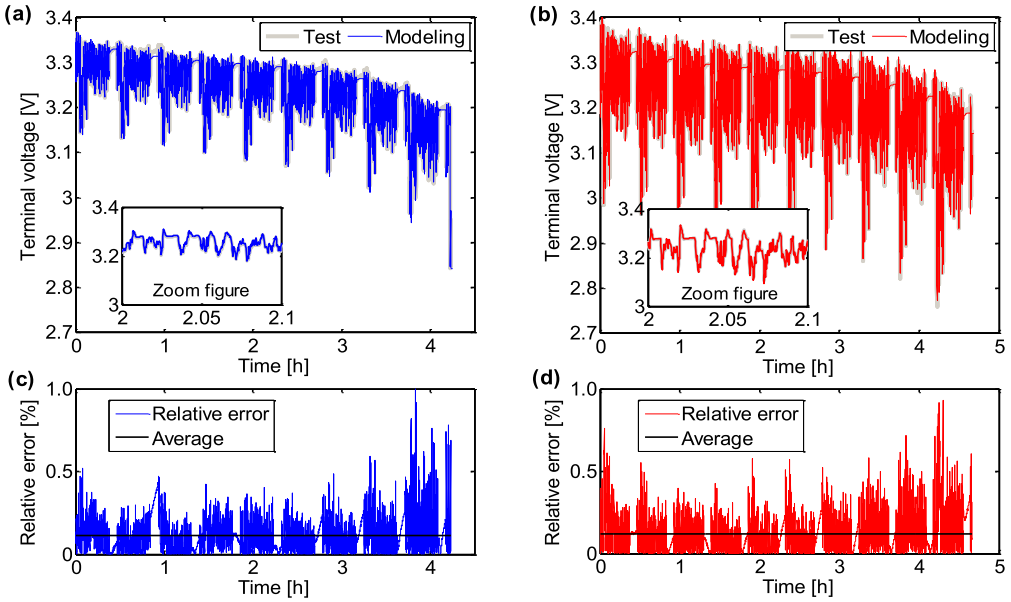

FIGURE 3. Modeling results of batteries in UDDS: (a) modeling of #1, (b) modeling of #2, (c) modeling relative error of #1, (d) modeling relative error of #2.

The charging and discharging power need to be promptly restricted when the SoC approaches the operational design limits. Assuming that the battery current is constant in the next time interval, the calculation should satisfy the following constraints:

$$\begin{cases} z_k - \dfrac{I_{L,k+T}\Delta t}{C} T\eta_d \geq z_{\min} & \text{if } I_{L,k+T} \geq 0 \\ z_k - \dfrac{I_{L,k+T}\Delta t}{C} T\eta_c \leq z_{\max} & \text{if } I_{L,k+T} < 0 \end{cases} \tag{7}$$

where η_c and η_d are the charging and discharging coulombic efficiency, respectively, $\eta_c = 0.98$ and $\eta_d = 1$, and $z_{\min}$ and $z_{\max}$ represent the lower boundary and upper boundary of the SoC operational design limits, respectively. In this study, the current is defined as positive when discharging while it is defined as negative when charging.

The operational current constraint is given by:

$$I_{\min} \leq I_{L,k+T} \leq I_{\max} \tag{8}$$

where $I_{\min}$ and $I_{\max}$ represent the lower boundary and upper boundary of the current operational design limits, respectively.

To avoid the risk of over-charging and over-discharging, the introduction of a voltage constraint for the SoP estimation is necessary. The voltage constraint can be expressed as:

$$\begin{cases} OCV(z_k - \dfrac{I_{L,k+T}\Delta t}{C} T\eta_d) - I_{L,k+T}R_{dis} \\ \times(z_k - \dfrac{I_{L,k+T}\Delta t}{C} T\eta_d) - U_{p,k+T} \geq U_{t\min} \quad \text{if } I_{L,k+T} \geq 0 \\ OCV(z_k - \dfrac{I_{L,k+T}\Delta t}{C} T\eta_c) - I_{L,k+T}R_{chg} \\ \times(z_k - \dfrac{I_{L,k+T}\Delta t}{C} T\eta_c) - U_{p,k+T} \leq U_{t\max} \quad \text{if } I_{L,k+T} < 0 \end{cases} \tag{9}$$

where $U_{t\min}$ and $U_{t\max}$ represent the lower bound and upper bound of the voltage operational design limits, respectively, and $U_{p,k+T}$ can be obtained by:

$$U_{p,k+T} = U_{p,k} e^{\frac{-T\Delta t}{\tau(z_k)}} + I_{L,k}R_p(z_k)\left(1 - e^{\frac{-\Delta t}{\tau(z_k)}}\right) \times \sum_{i=0}^{T-1} \left(e^{\frac{-\Delta t}{\tau(z_k)}}\right)^{T-1-i} \tag{10}$$

B. TAYLOR EXPANSION METHOD

The parameters OCV, R_{dis}, and R_{chg} in the model are the nonlinear functions of the current. A common used solution to resolve this problem is to linearize the function using the Taylor series expansion method (referred to as T-method) [7], [8], and [10].

The first-order Taylor series expansion is employed to express the future values of OCV:

$$\begin{cases} \text{for discharging:} \\ OCV(z_{k+1}) = OCV(z_k - \dfrac{I_{L,k+T}T\Delta t}{C}\eta_d) \\ = OCV(z_k) - \dfrac{I_{L,k+T}T\Delta t}{C}\eta_d \dfrac{\partial OCV(z)}{\partial z}\Big|_{z=z_k} + \Upsilon_1 \\ \text{for charging:} \\ OCV(z_{k+1}) = OCV(z_k - \dfrac{I_{L,k+T}T\Delta t}{C}\eta_c) \\ = OCV(z_k) - \dfrac{I_{L,k+T}T\Delta t}{C}\eta_c \dfrac{\partial OCV(z)}{\partial z}\Big|_{z=z_k} + \Upsilon_1 \end{cases} \tag{11}$$

where Υ_1 is the first-order residual which can be expressed

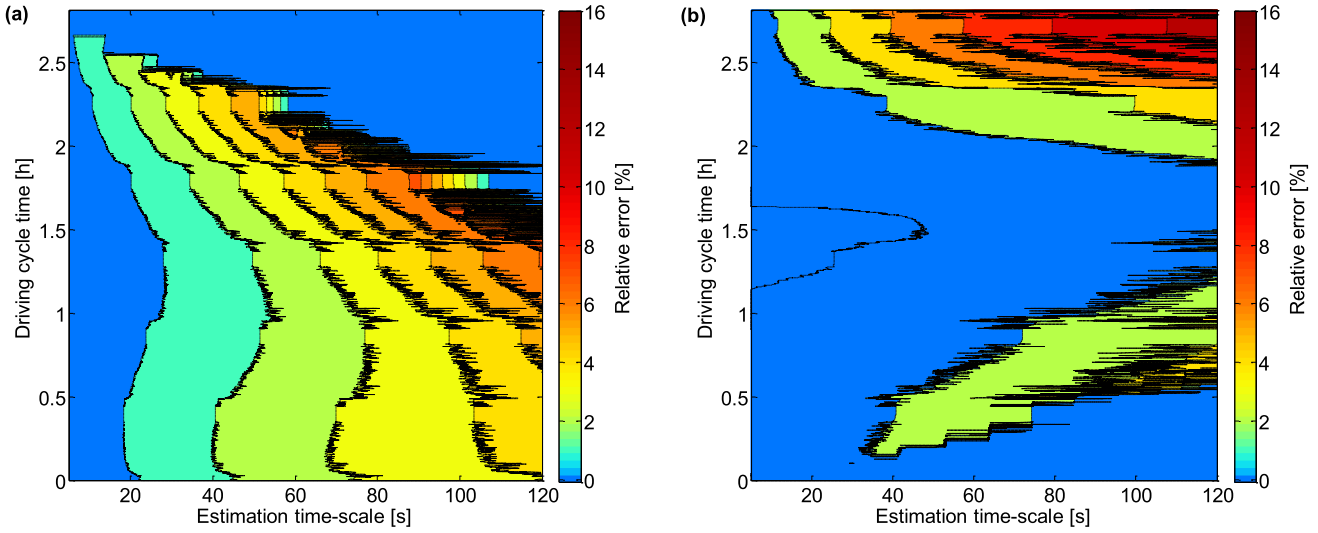

FIGURE 4. Influential map of Taylor series expansion at UDDS: (a) for discharging cases; (b) for charging cases.

in terms of Lagrange remainder:

$$\Upsilon_1 = \begin{cases} \text{for discharging:} \\ \frac{1}{2}\xi(I_{L,k+T})\frac{\partial^2 OCV(z)}{\partial z^2}\left(\frac{I_{L,k+T}T\Delta t}{C}\eta_d\right)^2 \\ \text{for charging:} \\ \frac{1}{2}\xi(I_{L,k+T})\frac{\partial^2 OCV(z)}{\partial z^2}\left(\frac{I_{L,k+T}T\Delta t}{C}\eta_c\right)^2 \end{cases} \tag{12}$$

where ξ is a number between z_k and z_{k+1}. It is assumed that the change of SoC is relatively small during T:

$$\begin{cases} \frac{I_{L,k+T}T\Delta t}{C}\eta_d \to 0 & \text{for discharging} \\ \frac{I_{L,k+T}T\Delta t}{C}\eta_c \to 0 & \text{for charging} \end{cases} \tag{13}$$

Therefore, the first-order residual can be generally omitted. The changes of R_{dis} and R_{chg} during T are ignored in T-method. From the Eq. (9) and Eq.(11), the maximum current can be expressed by:

$$\begin{cases} I_{\max}^{\text{dis,volt}} = \dfrac{OCV(z_k) - U_{p,k+T} - U_{t\min}}{R_{dis}(z_k) + \frac{\eta_d T\Delta t}{C}\frac{\partial OCV(z)}{\partial z}\big|_{z=z_k}} \\ I_{\min}^{\text{chg,volt}} = \dfrac{OCV(z_k) - U_{p,k+T} - U_{t\max}}{R_{chg}(z_k) + \frac{\eta_c T\Delta t}{C}\frac{\partial OCV(z)}{\partial z}\big|_{z=z_k}} \end{cases} \tag{14}$$

Based on Eq. (7), the maximum current constrained by SoC limitation can be expressed by:

$$\begin{cases} I_{\max}^{\text{dis,soc}} = \dfrac{C(z_k - z_{\min})}{T\eta_d\Delta t} \\ I_{\min}^{\text{chg,soc}} = \dfrac{C(z_k - z_{\max})}{T\eta_c\Delta t} \end{cases} \tag{15}$$

According to the T-method, battery is considered to provide the maximum power when the maximum allowed current is output. Thus, the SoP can be estimated by:

$$\begin{cases} P_{\max}^{dis} = n_s n_p I_{\max}^{\text{dis}} U_t(I_{\max}^{\text{dis}}) \\ P_{\min}^{chg} = n_s n_p I_{\min}^{\text{chg}} U_t(I_{\min}^{\text{chg}}) \end{cases} \tag{16}$$

where n_s is the number of cells connected in series in each module, n_p is the number of modules connected in parallel, $I_{\max}^{\text{dis}}$ and $I_{\max}^{\text{chg}}$ are the maximum allowed discharge and charge current solved by:

$$\begin{cases} I_{\max}^{\text{dis}} = \min(I_{\max}, I_{\max}^{\text{dis,volt}}, I_{\max}^{\text{dis,soc}}) \\ I_{\min}^{\text{chg}} = \max(I_{\min}, I_{\min}^{\text{chg,volt}}, I_{\min}^{\text{chg,soc}}) \end{cases} \tag{17}$$

C. DISCUSSION OF THE TAYLOR REMAINDER ERROR

The T-method is widely used and has been well evaluated as effective in battery state estimation, but it has some drawbacks. The Taylor expansion produces a remainder error; for long estimation time-scale, the remainder error may become large and cannot be neglected. To illustrate this issue, the SoP estimation is conducted based on T-method under UDDS driving cycles, which last about 2.5 hours to allow the battery charge depletes from 100% to 10%. Fig. 4 shows the calculated remainder error in Taylor expansion of the SoP estimation for LiB with different time-scales. Obviously, at each time point, the Taylor remainder error becomes larger with the increase of estimation time-scale in both charging and discharging situation. It can also be noticed that the situation gets worse at terminal phase of the driving cycle. This is due to the high nonlinearity of OCV at low SoC region.

Normally, there are two solutions to reduce the remainder error, one is using high order Taylor expansion, second is setting short time-scale. However, too short time-scale is not suitable for online update in real-time control. Especially in electric vehicle power management application, the estimation of continuous maximum power ability lasting for a

certain period of time is usually crucial for the controller to determine the power allocation in the future.

D. GA-BASED SoP ESTIMATION

Based on the above analysis, an improved GA-based SoP estimation strategy is proposed for power management application. The presented method is suitable for long time-scale estimation and is not impacted by the model complexity. GA is employed to obtain the value of the current that corresponds to the maximum power of LiB, thus, the SoP estimation can be treated as an optimization problem. Here the discharge and charge process are treated separately. For the cases of discharging ($I_{L,k+T} \geq 0$), the optimization objective and constraints are expressed by:

$$\max \left[I_{L,k+T} \begin{pmatrix} OCV(z_k - \dfrac{I_{L,k+T}\Delta t}{C} T\eta_d) \\ -I_{L,k+T} R_{dis}(z_k - \dfrac{I_{L,k+T}\Delta t}{C} T\eta_d) \\ -U_{p,k+T} \end{pmatrix} \right]$$

$$s.t. \begin{cases} S_{d1} : 0 \leq I_{L,k+T} \leq I_{\max} \\ S_{d2} : z_k - \dfrac{I_{L,k+T}\Delta t}{C} T\eta_d \geq z_{\min} \\ S_{d3} : OCV(z_k - \dfrac{I_{L,k+T}\Delta t}{C} T\eta_d) \\ -I_{L,k+T} R_{dis}(z_k - \dfrac{I_{L,k+T}\Delta t}{C} T\eta_d) - U_{p,k+T} \geq U_{t\min} \end{cases} \tag{18}$$

where S_{d1}, S_{d2} and S_{d3} are logical values of each constraint for discharging cases.

For cases of charging ($I_{L,k+T} < 0$), the optimization objective and constraints are expressed by:

$$\min \left[I_{L,k+T} \begin{pmatrix} OCV(z_k - \dfrac{I_{L,k+T}\Delta t}{C} T\eta_c) \\ -I_{L,k+T} R_{chg}(z_k - \dfrac{I_{L,k+T}\Delta t}{C} T\eta_c) \\ -U_{p,k+T} \end{pmatrix} \right]$$

$$s.t. \begin{cases} S_{c1} : I_{\min} \leq I_{L,k+T} \leq 0 \\ S_{c2} : z_k - \dfrac{I_{L,k+T}\Delta t}{C} T\eta_c \leq z_{\max} \\ S_{c3} : OCV(z_k - \dfrac{I_{L,k+T}\Delta t}{C} T\eta_c) \\ -I_{L,k+T} R_{chg}(z_k - \dfrac{I_{L,k+T}\Delta t}{C} T\eta_c) - U_{p,k+T} \leq U_{t\max} \end{cases} \tag{19}$$

where S_{c1}, S_{c2} and S_{c3} are defined as a logical value of each constraint for charging cases.

The employed GA is described as follows:

1) INITIALIZATION

Float code is employed and the current constraints are set as the bounds of the optimization variable. The population size can be considered as an n-vector P_n:

$$P_n = [c_1 \quad c_2 \quad \dots \quad c_n] \tag{20}$$

where $c_1 \sim c_n$ represent the individuals of the population.

The initial individuals are randomly generated according to the population size. To improve the searching performance, the initial individuals are set as:

$$\begin{cases} c_i = (i-1)\dfrac{I_{\max}}{n-1} & (i = 1, 2, \dots, n) \text{ for discharging} \\ c_i = (i-1)\dfrac{I_{\min}}{n-1} & (i = 1, 2, \dots, n) \text{ for charging} \end{cases} \tag{21}$$

2) FITNESS EVALUATION

The fitness function, which is used to measure the quality for all individuals, is established as follows:

$$J_d = \begin{cases} \text{if } S_{d2} \wedge S_{d3} = 1 : \\ I_{L,k+T} \begin{pmatrix} OCV(z_k - \dfrac{I_{L,k+T}\Delta t}{C} T\eta_d) \\ -I_{L,k+T} R_{dis}(z_k - \dfrac{I_{L,k+T}\Delta t}{C} T\eta_d) \\ -U_{p,k+T} \end{pmatrix} \\ \text{if } S_{d2} \wedge S_{d3} = 0 : \\ \lambda_d I_{L,k+T} \begin{pmatrix} OCV(z_k - \dfrac{I_{L,k+T}\Delta t}{C} T\eta_d) \\ -I_{L,k+T} R_{dis}(z_k - \dfrac{I_{L,k+T}\Delta t}{C} T\eta_d) \\ -U_{p,k+T} \end{pmatrix} \end{cases} \tag{22}$$

$$J_c = \begin{cases} \text{if } S_{c2} \wedge S_{c3} = 1 : \\ I_{L,k+T} \begin{pmatrix} OCV(z_k - \dfrac{I_{L,k+T}\Delta t}{C} T\eta_c) \\ -I_{L,k+T} R_{chg}(z_k - \dfrac{I_{L,k+T}\Delta t}{C} T\eta_c) \\ -U_{p,k+T} \end{pmatrix} \\ \text{if } S_{c2} \wedge S_{c3} = 0 : \\ \lambda_c I_{L,k+T} \begin{pmatrix} OCV(z_k - \dfrac{I_{L,k+T}\Delta t}{C} T\eta_c) \\ -I_{L,k+T} R_{chg}(z_k - \dfrac{I_{L,k+T}\Delta t}{C} T\eta_c) \\ -U_{p,k+T} \end{pmatrix} \end{cases} \tag{23}$$

where λ_d and λ_c represent the penalty factors to replace the multiple constraints.

Considering that the fitness function is required to be nonnegative, the fitness functions are rewritten as:

$$F(I_{L,k+T}) = \begin{cases} J_d(I_{L,k+T}) & \text{for discharging cases} \\ -J_c(I_{L,k+T}) & \text{for charging cases} \end{cases} \tag{24}$$

3) SELECTION

The higher fitness value has the higher probability to remain in the next generation. This can be achieved by the roulette strategy, in which the area of each segment is proportional to the fitness value of the individual. Then, the algorithm selects one of the sections randomly. However, this process probably destroys the individual genes with the highest fitness, and influences the convergence quality of the algorithm. To address this problem, the elitist strategy is used to exclude some of the great individuals (elites) from the roulette game and copy them directly to the next generation to ensure that every elite in each generation can survive in priority.

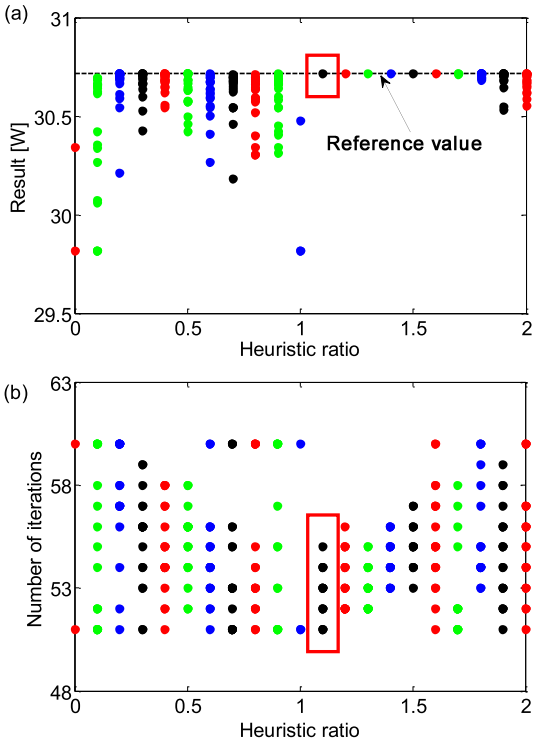

FIGURE 5. Results of 20 discharge SoP estimation tests at different heuristic ratio: (a) calculation result; (b) number of iterations.

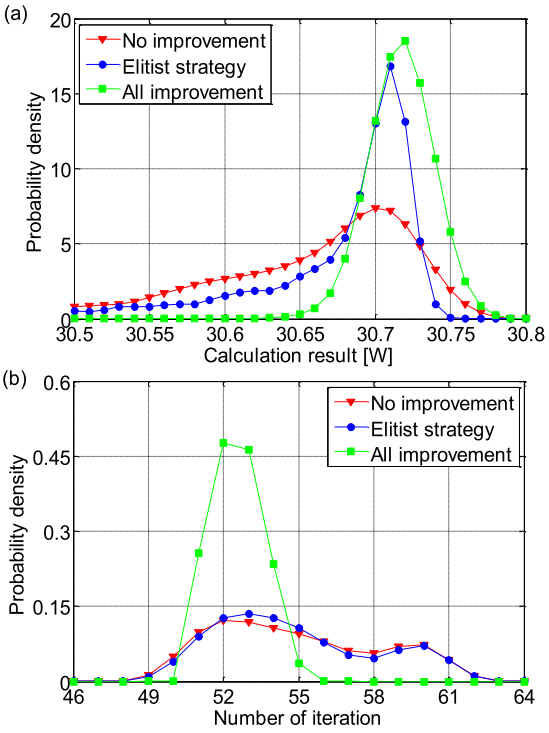

FIGURE 6. Statistical results of 200 discharge SoP estimation tests with different improvements: (a) probability distribution of estimation results; (b) probability distribution of reproduction times.

4) GENERATING NEW INDIVIDUALS

After selection, the selected individuals will undergo crossover and mutation operations to generate new individuals. The crossover operator can combine two individuals to form a new individual. The mutation operator can exert a small change in the individuals, which provides the genetic density. To improve the convergence speed, a heuristic crossover operator is used here to guide the offspring to the direction of the good parents. Heuristic ratio is an important parameter that determines the degree of the parents' guidance to the offspring. The heuristic ratio is generally between 0 and 2. To choose a reasonable value, we perform 20 discharge SoP estimation tests on cell #1 under different heuristic ratios, as shown in Fig. 5. As shown in Fig. 5 (a), the algorithm can achieve a stable convergence around the reference value when the heuristic ratio is between 1.1 and 1.7. Fig. 5 (b) shows that the number of iterations is relatively small and stable when the heuristic ratio is 1.1. Thus, the heuristic ratio is set as 1.1 here.

The fitness value of the best individual can be obtained at each iteration step, and the objective function value of the best individual can be deduced from Eq. (24). Then, the battery SoP can be calculated by the following expressions:

$$\begin{cases} P_{\max}^{dis} = n_s n_p J_d^* \\ P_{\min}^{chg} = n_s n_p J_c^* \end{cases} \tag{25}$$

where J_d^* and J_c^* are the objective function values of the best individual from GA.

TABLE 1. Operational design limits for the battery cell.

Parameter	Minimum	Maximum
SoC	0.2	0.9
I_L (A)	-27	27
U_t (V)	2.5	3.65

To verify the effectiveness of the improvements, 200 discharge SoP estimation tests with different improvements are carried out, and the statistical results of the tests are shown in Fig. 6. The probability density is based on kernel density estimation. It is seen in Fig. 6 (a) that the improvements promote the rise and right shift of the wave peak, and the calculation results tend to be concentrated. This indicates that two improvements improve the convergence quality of GA, among which the elitist strategy is the main contribution. From Fig. 6 (b), the introduction of heuristic crossover significantly stabilized the number of iterations at a lower level.

IV. RESULTS AND DISCUSSION

The performance of the presented GA-based SoP estimation method is evaluated by a simulation study and is compared with the T-method. Here, a battery pack composed by 20 cells in series is adopted. The operation limits of the LiB cells are given in Table 1. The main parameters of the GA-based method are summarized in Table 2.

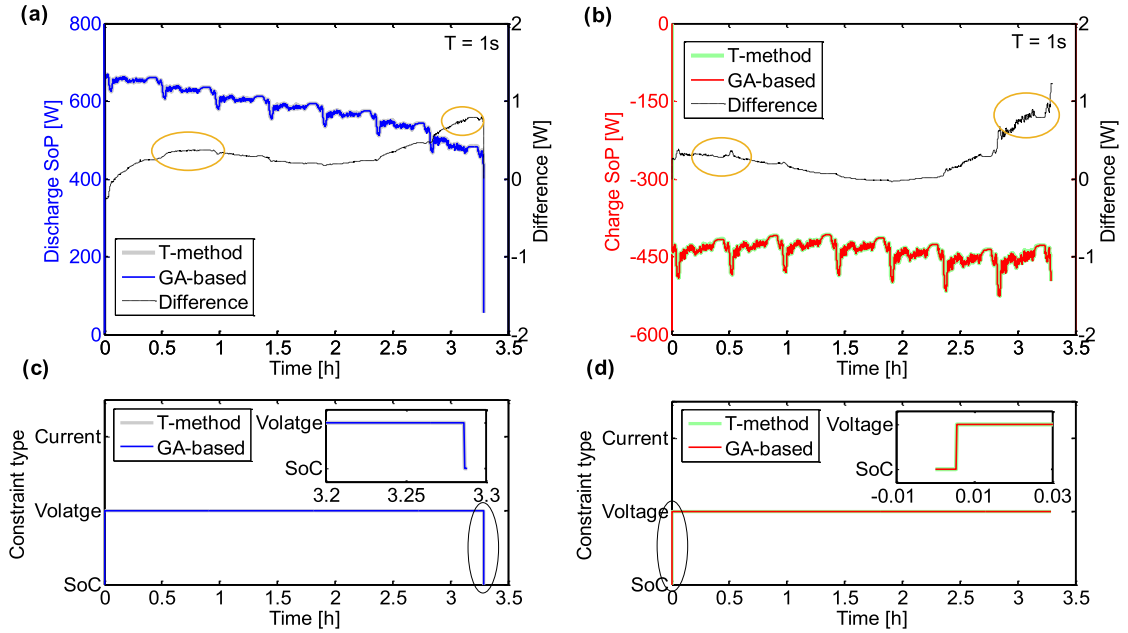

FIGURE 7. SoP estimation results of the T-method and the GA-based method with $T = 1$ s at UDDS: (a) discharge SoP with both methods and the estimation difference; (b) charge SoP with both methods and the estimation difference; (c) active constraint type for the discharge SoP; (d) active constraint type for the charge SoP.

TABLE 2. The parameters of GA.

Name	Value
Population size	100
Generation	50
Encoded mode	Float
Mutation function	Uniform
Mutation rate	0.01
Crossover function	Heuristic
Crossover ratio	1.1
Average change	1e-15
Values of λ_c	500
Values of λ_d	500

Fig. 7 shows the comparison between GA-based method and T-method method with a short time-scale ($T = 1$ s), where the difference between these two methods are also indicated. The estimation results of both methods are quite approaching because the remainder error of Taylor expansion is relatively small at such situation. From Fig. 7 (c) and Fig. 7 (d), the active constraints of both methods are also very consistent. Both methods can achieve good performances for the instantaneous estimation time-scale. Note that the differences are relatively high in the periods of beginning and ending, which are marked in the figure. This is because the OCV and internal resistance have higher nonlinearities during these periods, but the GA-based method is not impacted by the nonlinearities. The T-method leads to a slight overestimation for discharging cases but a slight underestimation for charging cases.

Fig. 8 shows the results of SoP estimation with a long time-scale ($T = 30$ s). From the comparison, the differences between GA-based method and T-method in Fig. 8 are much larger than that in Fig. 7. This result illustrates the Taylor expansion in T-method are not suitable for estimation with the long estimation time-scale. From the Fig. 8 (a) and Fig. 8 (b), it can be seen that the maximum relative deviation is up to 4.3% for the discharging process and is up to 7.2% for the charging process. Fig. 8 (a) and Fig. 8 (c) show that the deviation mainly occurs at the voltage constraint. The Taylor expansion of the T-method only affects the estimation at the voltage constraint. The overestimation of the T-method leads to an early trigger of the SoC constraint for the discharging case. In Fig. 8 (b) and Fig. 8 (d), the underestimation of the T-method leads to an early trigger of the voltage constraint for the charging case. In cases of continuous long estimation time-scale, the GA-based method gains a better performance of SoP estimation.

If the estimation time-scale is further extended, some extreme situations for the SoP estimation probably arise. Here, a possible extreme situation is deliberately simulated to illustrate the existence of extreme cases, where the SoC constraint is adjusted to [0.1, 1]. This simulated case occurs when the cell is fully charged with an instantaneous current −9.45 A (7C). Then, the two SoP estimation algorithms are performed at this moment to estimate the discharge SoP with $T = 225$ s. The characteristic of battery output power at this moment and the SoP estimation results of the two methods are described in Fig. 9. It is seen that a large difference has emerged in the estimation results of both methods, where the GA-based method is more closely approximated to the maximum battery output power characteristic. Notice that the T-method has led to failure of the voltage constraint, where the ideal solution of the T-method has been marked in the figure. The reason for the failure is that the error

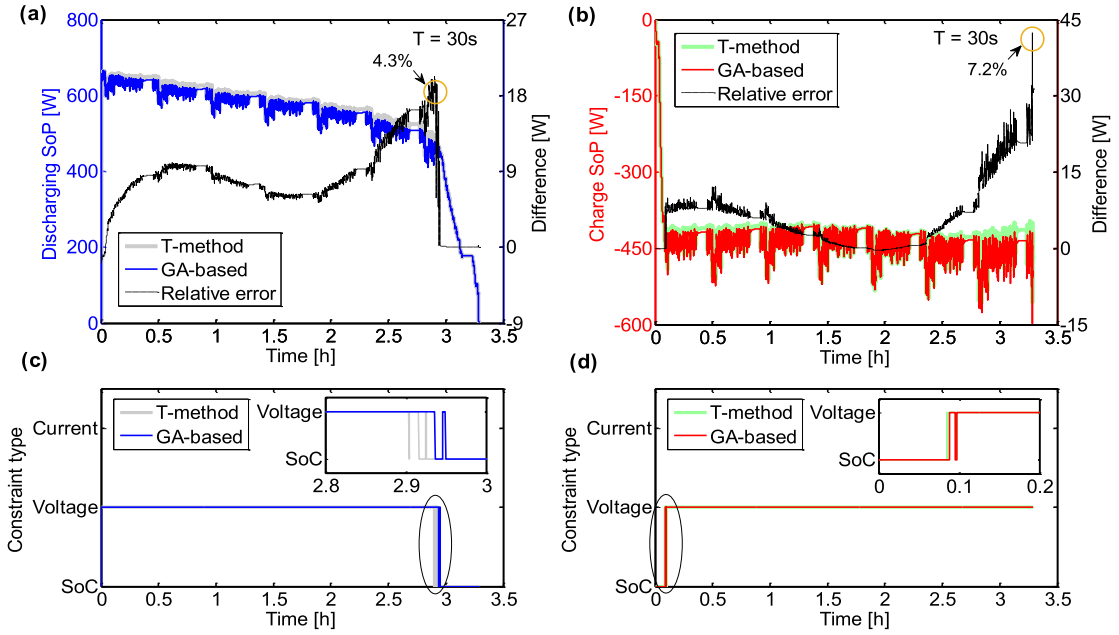

FIGURE 8. SoP estimation results of the T-method and the GA-based method with $T = 30$ s at UDDS: (a) discharge SoP with both methods and the estimation difference; (b) charge SoP with both methods and the estimation difference; (c) active constraint type for the discharge SoP; (d) active constraint type for the charge SoP.

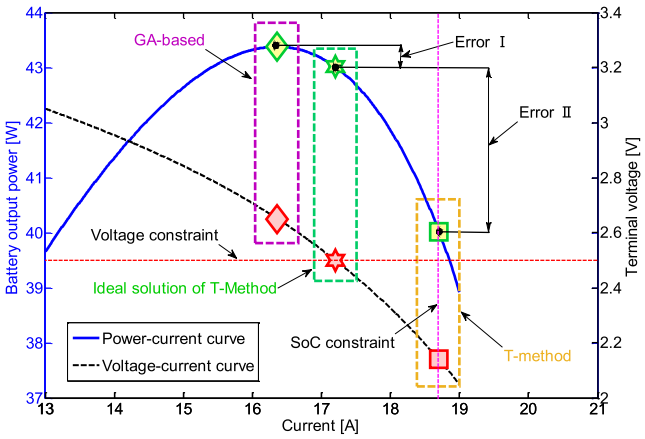

FIGURE 9. Characteristics of the battery cell output power and SoP estimation results of both methods.

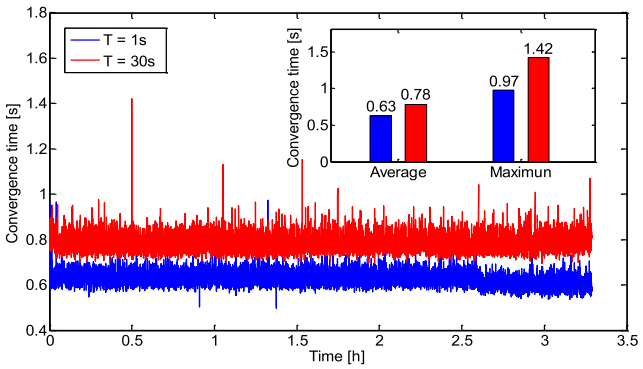

FIGURE 10. Convergence time of GA-based method with $T = 1$ s and $T = 30$ s at UDDS.

of the Taylor series expansion is further enlarged in this long estimation time-scale, which decreased the acceptance linearization deviation. This error leads to an overestimation of the maximum current, which triggers the SoC constraint in advance. Further, from Fig. 9 we can find that the ideal solution of the T-method is still biased with the maximum of the power characteristics. This is because the battery output power characteristic is not monotonic, as described in Fig. 9. For the GA-based method, due to the optimization of the GA, this problem has been effectively solved. However, the estimating process of the T-method does not take this into account. As a consequence, the deviation between the two methods can be divided into two parts, represented in the Fig. 9 as error I and error II. The first is caused by the linear approximation; the second is caused by neglecting the variation of the battery output power. Therefore, the GA-based method is more accurate for the SoP estimation due to the above considerations. The convergence time of GA-based SoP estimation is shown in Fig. 10. For long estimation time-scale (30s), the average convergence time of the algorithm is less than 1.42 s. This time period is much shorter than the time-scale. Concerning the variation of battery SoP is not volatile in such a short time, the presented algorithm is available in the real-time power management of electric vehicle applications.

V. INFLUENCE ANALYSIS OF IMPRECISE SOC

The implementation of SoP estimation relies on the battery SoC information; however, precisely estimating SoC error

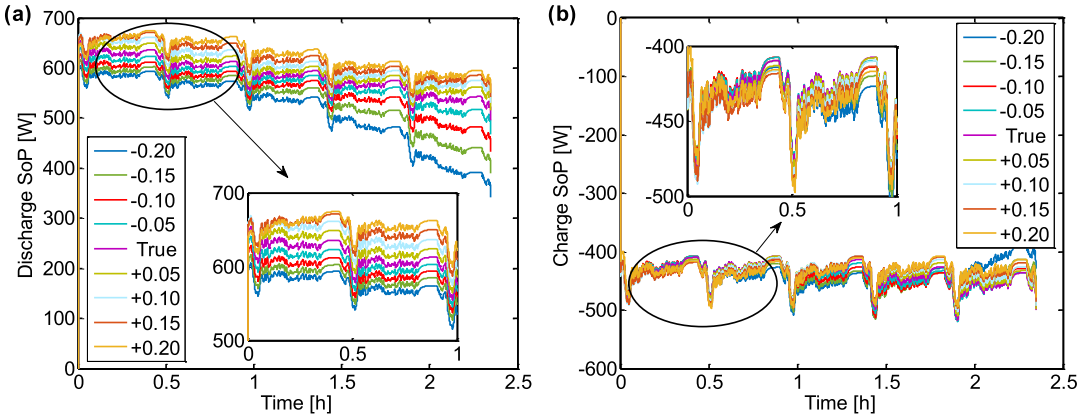

FIGURE 11. Imprecise estimation results of battery pack of cell #1 with T = 1 s at UDDS: (a) imprecise results of discharge SoP (b) imprecise results of charge SoP.

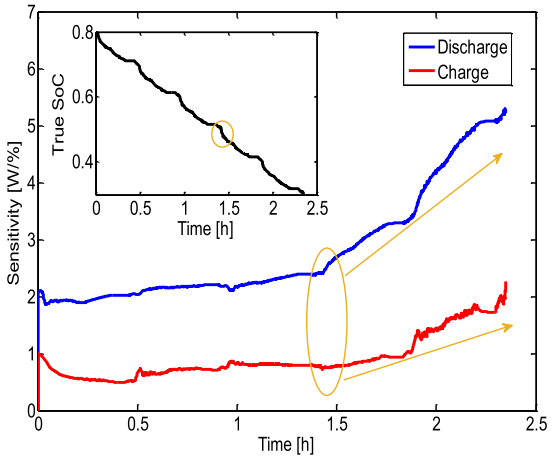

FIGURE 12. Sensitivity δ of the battery pack of cell #1 with $T = 1$ s at UDDS and the true SoC value.

remains a very difficult task at current [23]. In this section, the influence of imprecise SoC information on SoP estimation is discussed. We will temporarily not consider the SoC constraint but will instead focus on the influence of imprecise SoC information on the presented SoP estimation algorithm with voltage and current constraints.

A. SENSITIVITY COEFFICIENT OF IMPRECISE SoC

A sensitivity coefficient δ of SoC accuracy is introduced here to reflect the impact of the SoC error on the battery SoP estimation, expressed by:

$$\delta = \frac{\sum_{j=1}^{N-1} \left| \left(P_{j+1} - P_j\right) / \left(z_{j+1} - z_j\right) \right|}{100N} \tag{26}$$

where N is the total of the artificial certain SoC errors (including zero error), such as the above eight imprecise SoC values and one true SoC value. these values are then sequenced according to the magnitude of the error value, P_j represents the j-th wrong SoP value caused by the j-th imprecise SoC value z_j.

Eight certain SoC errors in the range of -0.2 to 0.2 are artificially exerted into the SoP estimation process. The imprecise estimation results of the battery pack of cell #1 ($n_s = 20$, $n_p = 1$) with $T = 1$ s at UDDS are shown in Fig. 11, where the purple curves represent the correct estimation results. It is seen that the SoP estimation of the charge and discharge are affected in varying degrees by the SoC errors. By combining Fig. 11 (a) and Fig. 11 (b), we can find that the SoP estimation for the discharging case is more sensitive to the SoC errors. The δ calculation of the battery pack of cell #1 with $T = 1$ s at UDDS is shown in Fig. 12. It can be seen that the variation of δ with time exhibits a rising trend. After approximately 1.5 hours, the rising trend is larger. When the SoC reaches the low level, the δ is notably sensitive to the SoC error, indicating that the impact of imprecise SoC information on SoP estimation gets larger with the decrease of SoC.

B. INFLUENCE OF SoH

The previous analyses are based on the battery characteristic. When battery gets aging, the battery characteristic and its model would be changed. The coefficient δ is also impacted by the battery SoH. To investigate the correlation of δ with varying SoH, a battery pack of cell #2, which represents an aged state, is employed to perform the imprecise SoP estimation with $T = 1$ s at UDDS. The estimation results compared with a battery pack of cell #1 are shown in Fig. 13. Based on the results, the δ can be calculated, as described in Fig. 14.

The result shows that the δ decline significantly when battery is aging. From the comparison of the mean value, the average δ decreased by more than 50% due to the battery aging. This is mainly because the battery internal resistance increases and the battery power capability declines during the aging process. When the battery gets aging, the tendency of δ to change become more subdued, and its standard deviation (SD) decreases to a very low level. This indicates that the δ will become more insensitive to the SoC level after aging. Therefore, the influence of the SoC error on the

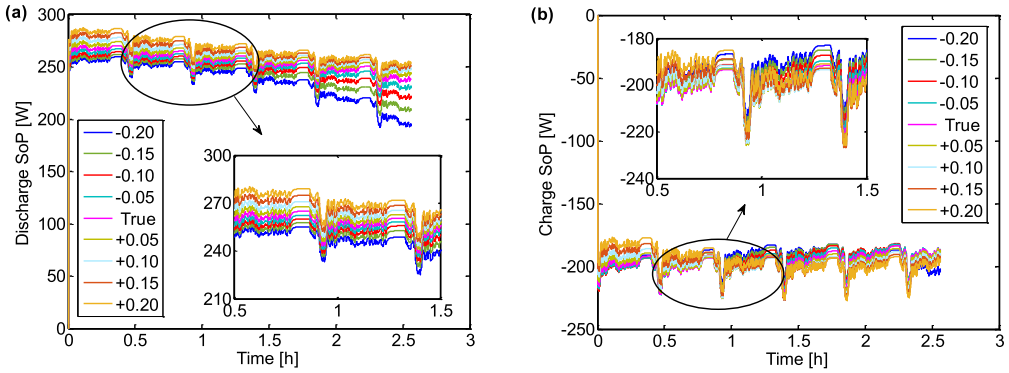

FIGURE 13. Imprecise estimation results of the battery pack of cell #2 with $T = 1$ s at UDDS: (a) imprecise results of the discharge SoP; (b) imprecise results of the charge SoP.

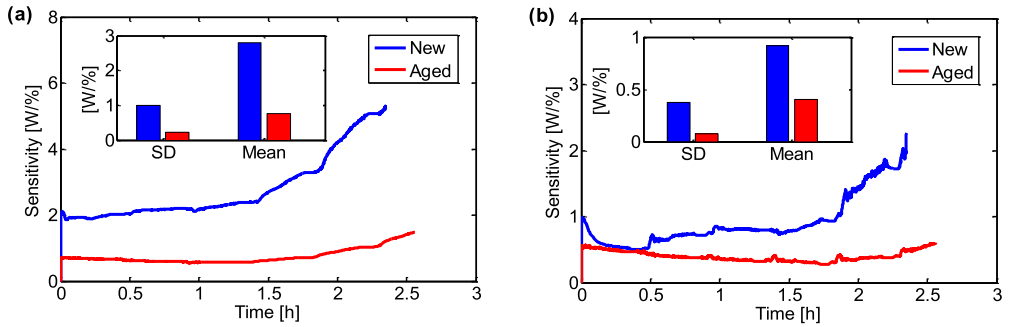

FIGURE 14. Sensitivities δ of varying SoH with $T = 1$ s at UDDS: (a) results for discharge SoP; (b) results for charge SoP.

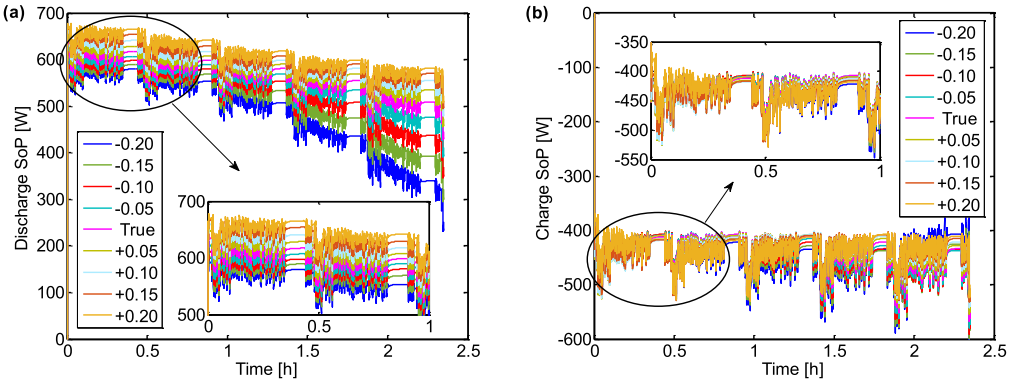

FIGURE 15. Imprecise estimation results of the battery pack of cell #1 with $T = 30$ s at UDDS: (a) imprecise results of the discharging SoP; (b) imprecise results of the charging SoP.

SoP estimation is quite minor for the aging battery in comparison of that for healthy battery.

C. INFLUENCE OF ESTIMATION TIME-SCALE

To investigate the correlation of δ with the varying estimation time-scale, the battery pack of cell #1 is employed to perform the imprecise SoP estimation with $T = 30$ s at UDDS. The estimation results compared with $T = 1$ s are shown in Fig. 15. The variation of coefficient δ is plotted in Fig. 16. From the comparison between Fig. 14 and Fig. 16, it can be noticed that the impact on δ caused by varying time-scale is smaller than that caused by SoH. In Fig. 16 (a), the value of δ with long time-scale is higher than that with short time-scale in general. δ is enlarged after the time is over 1 h, indicating that the longer estimation time-scale leads to a slightly higher sensitivity of the discharge SoP estimation to the SoC error at low SoC area. On the contrary, when SoC is at high area, the sensitivity of SoP to SoC accuracy is not affected by the estimation time-scale. In Fig. 16 (b), the value of δ shows a slight drop on the whole, which shows that the long time-scale leads to lower sensitivity of the discharge SoP estimation to the SoC error.

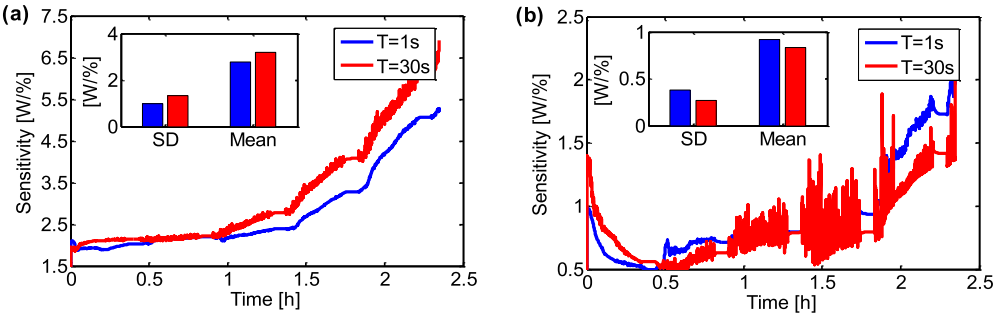

FIGURE 16. Sensitivities δ at the varying estimation time-scale: (a) for case of discharging; (b) for case of charging.

VI. CONCLUSION

In this study, a GA-based method of SoP estimation is proposed for LiBs in electric vehicles concerning the influence of imprecise SoC information. The presented approach can deal with the problem of big remainder error in Taylor expansion under large estimation time-scale. Simulation results indicate the GA-based method can improve the estimation accuracy of the SoP by up to 7.2% under certain situations. A sensitivity coefficient of the SoP estimation to the SoC error is introduced. The impact of battery SoH and estimation time-scale on the sensitivity coefficient has been analyzed.

REFERENCES

[1] A. Fotouhi, D. J. Auger, K. Propp, S. Longo, and M. Wild, "A review on electric vehicle battery modelling: From Lithium-ion toward Lithium–Sulphur," *Renew. Sustain. Energy Rev.*, vol. 56, pp. 1008–1021, Apr. 2016.

[2] M. A. Hannan, F. A. Azidin, and A. Mohamed, "Hybrid electric vehicles and their challenges: A review," *Renew. Sustain. Energy Rev.*, vol. 29, pp. 135–150, Jan. 2014.

[3] H. He, R. Xiong, H. Guo, and S. Li, "Comparison study on the battery models used for the energy management of batteries in electric vehicles," *Energy Conversion Manage.*, vol. 64, pp. 113–121, Dec. 2012.

[4] X. Ding *et al.*, "Analytical and experimental evaluation of SiC-inverter nonlinearities for traction drives used in electric vehicles," *IEEE Trans. Veh. Technol.*, vol. 67, no. 1, pp. 146–159, Jan. 2017.

[5] J. Jaguemont, L. Boulon, and Y. Dube, "Characterization and modeling of a hybrid-electric-vehicle lithium-ion battery pack at low temperatures," *IEEE Trans. Veh. Technol.*, vol. 65, no. 1, pp. 1–14, Jan. 2016.

[6] F. Zheng, J. Jiang, B. Sun, W. Zhang, and M. Pecht, "Temperature dependent power capability estimation of lithium-ion batteries for hybrid electric vehicles," *Energy*, vol. 113, pp. 64–75, Oct. 2016.

[7] X. Hu, R. Xiong, and B. Egardt, "Model-based dynamic power assessment of lithium-ion batteries considering different operating conditions," *IEEE Trans. Ind. Informat.*, vol. 10, no. 3, pp. 1948–1959, Aug. 2014.

[8] R. Xiong, H. He, F. Sun, and K. Zhao, "Online estimation of peak power capability of Li-Ion batteries in electric vehicles by a hardware-in-loop approach," *Energies*, vol. 5, no. 5, pp. 1455–1469, 2012.

[9] S. Wang, M. Verbrugge, J. S. Wang, and P. Liu, "Multi-parameter battery state estimator based on the adaptive and direct solution of the governing differential equations," *J. Power Sour.*, vol. 196, no. 20, pp. 8735–8741, 2011.

[10] S. Wang, M. Verbrugge, J. S. Wang, and P. Liu, "Power prediction from a battery state estimator that incorporates diffusion resistance," *J. Power Sour.*, vol. 214, pp. 399–406, Sep. 2012.

[11] W. Waag, C. Fleischer, and D. U. Sauer, "Critical review of the methods for monitoring of lithium-ion batteries in electric and hybrid vehicles," *J. Power Sour.*, vol. 258, pp. 321–339, Jul. 2014.

[12] A. Farmann and D. U. Sauer, "A comprehensive review of on-board state-of-available-power prediction techniques for lithium-ion batteries in electric vehicles," *J. Power Sour.*, vol. 329, pp. 123–137, Oct. 2016.

[13] W. Waag, C. Fleischer, and D. U. Sauer, "Adaptive on-line prediction of the available power of lithium-ion batteries," *J. Power Sour.*, vol. 242, pp. 548–559, Nov. 2013.

[14] D. Kim and D. Jung, "Method of estimating maximum output of battery for hybrid electric vehicle," U.S. Patent 7 518 375 B2, Apr. 14. 2009.

[15] G. L. Plett, "High-performance battery-pack power estimation using a dynamic cell model," *IEEE Trans. Veh. Technol.*, vol. 53, no. 5, pp. 1586–1593, Sep. 2004.

[16] F. Sun, R. Xiong, H. He, W. Li, and J. E. E. Aussems, "Model-based dynamic multi-parameter method for peak power estimation of lithium–ion batteries," *Appl. Energy*, vol. 96, pp. 378–386, Aug. 2012.

[17] R. Xiong, F. Sun, H. He, and T. Nguyen, "A data-driven adaptive state of charge and power capability joint estimator of lithium-ion polymer battery used in electric vehicles," *Energy*, vol. 63, pp. 295–308, Dec. 2013.

[18] L. Wang, Y. Cheng, and J. Zou, "Battery available power prediction of hybrid electric vehicle based on improved Dynamic Matrix Control algorithms," *J. Power Sour.*, vol. 261, pp. 337–347, Sep. 2014.

[19] T. Feng, L. Yang, X. Zhao, H. Zhang, and J. Qiang, "Online identification of lithium-ion battery parameters based on an improved equivalent-circuit model and its implementation on battery state-of-power prediction," *J. Power Sour.*, vol. 281, pp. 192–203, May 2015.

[20] G. Dong, J. Wei, and Z. Chen, "Kalman filter for onboard state of charge estimation and peak power capability analysis of lithium-ion batteries," *J. Power Sour.*, vol. 328, pp. 615–626, Oct. 2016.

[21] W. Zhan, W. Shi, and Z. Ma, "Adaptive unscented Kalman filter based state of energy and power capability estimation approach for lithium-ion battery," *J. Power Sour.*, vol. 289, pp. 50–62, Sep. 2015.

[22] L. Pei, C. Zhu, T. Wang, R. Lu, and C. C. Chan, "Online peak power prediction based on a parameter and state estimator for lithium-ion batteries in electric vehicles," *Energy*, vol. 66, pp. 766–778, Mar. 2014.

[23] S. Mohan, Y. Kim, and A. G. Stefanopoulou, "Estimating the power capability of Li-ion batteries using informationally partitioned estimators," *IEEE Trans. Control Syst. Technol.*, vol. 24, no. 5, pp. 1643–1654, Sep. 2016.

[24] Y. Wang, R. Pan, C. Liu, Z. Chen, and Q. Ling, "Power capability evaluation for lithium iron phosphate batteries based on multi-parameter constraints estimation," *J. Power Sour.*, vol. 374, pp. 12–23, Jan. 2018.

[25] P. Malysz, J. Ye, R. Gu, H. Yang, and A. Emadi, "Battery state-of-power peak current calculation and verification using an asymmetric parameter equivalent circuit model," *IEEE Trans. Veh. Technol.*, vol. 65, no. 6, pp. 4512–4522, Jun. 2016.

[26] T. Wik, B. Fridholm, and H. Kuusisto, "Implementation and robustness of an analytically based battery state of power," *J. Power Sour.*, vol. 287, pp. 448–457, Aug. 2015.

[27] C. Burgos-Mellado, M. E. Orchard, M. Kazerani, R. Cárdenas, and D. Sáez, "Particle-filtering-based estimation of maximum available power state in Lithium-Ion batteries," *Appl. Energy*, vol. 161, pp. 349–363, Jan. 2016.

[28] R. Xiong, H. He, F. Sun, X. Liu, and Z. Liu, "Model-based state of charge and peak power capability joint estimation of lithium-ion battery in plug-in hybrid electric vehicles," *J. Power Sour.*, vol. 229, pp. 159–169, May 2013.

[29] F. Sun, R. Xiong, and H. He, "Estimation of state-of-charge and state-of-power capability of lithium-ion battery considering varying health conditions," *J. Power Sour.*, vol. 259, pp. 166–176, Aug. 2014.

JIAHUAN LU received the B.S. degree in vehicle engineering from Northeastern University, Shenyang, China, in 2014, where he is currently pursuing the M.S. degree in automobile engineering. He is currently a Visiting Scholar with the State Key Laboratory of Automotive Simulation and Control, Changchun, China. His research mainly focuses on battery management system for electric vehicle applications.

ZEYU CHEN received the B.S. and M.S. degrees in automobile engineering from Jilin University, Changchun, China, in 2004 and 2007, respectively, and the Ph.D. degree from the Beijing Institute of Technology, Beijing, China, in 2010.

He is currently an Associate Professor in vehicle engineering with the School of Mechanical Engineering and Automation, Northeastern University, China. He is also a Visiting Scholar with the State Key Laboratory of Automotive Simulation and Control, Changchun, China. His research interests include the battery safety and battery management for electric vehicle applications, and the optimal control in power management of hybrid electric system.

YING YANG received the M.S. degree from the University of Manchester, Manchester, U.K., in 2003, and the Ph.D. degree in automobile engineering from Northeastern University, Shenyang, China, in 2000.

She is currently a Professor in vehicle engineering with the School of Mechanical Engineering and Automation, Northeastern University, China. Her research interests mainly include vehicle intelligent safety, vehicle dynamic control, and vehicle amenity design.

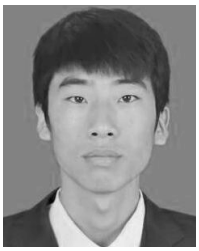

MING LV received the B.S. degree in vehicle engineering from Guizhou University, Guizhou, China, in 2014. He is currently pursuing the M.S. degree in automobile engineering with Northeastern University, Shenyang, China.

His research mainly focuses on control strategy and simulation for hybrid electric vehicles.